2-aminopurine as a probe for quadruplex loop structures

Published in final edited form as:
Methods Mol Biol. 2010 ; 608: 121–136. doi:10.1007/978-1-59745-363-9_8.

2-Aminopurine as a Probe for Quadruplex Loop Structures

Robert D. Gray, **Luigi Pettracone**, **Robert Buscaglia**, and **Jonathan B. Chaires***
James Graham Brown Cancer Center, University of Louisville, 529 S. Jackson St., Louisville, KY 40202

Summary

Fluorescent reporter groups have served for many years as sensitive probes of macromolecular structure. Such probes can be especially useful in comparative studies such as detection of conformational changes and discrimination among structural models. Spectroscopic methods such as fluorescence are attractive because they are rapid, require small amounts of material, are non-destructive, can be carried out with commonly available equipment, and are relatively inexpensive. In addition, there is a rich library of theoretical and practical materials available to aid in data interpretation. The intrinsic fluorescence of most nucleic acids is too low to be useful in structural studies. Thus, it is necessary to incorporate a suitable reporter group to utilize fluorescence methods involving polynucleotide structure. A highly fluorescent adenine analog, 2-aminopurine, has long served in this capacity. The present article describes our use of 2-aminopurine as a probe of loop structures in quadruplex DNA. In particular, we show how knowledge of the relative intensity of 2-aminopurine emission as well as its sensitivity to exogenous quenching molecules such as acrylamide can aid in comparing crystal and solution structures of an oligonucleotide model of the human telomere and in discrimination among models containing tandem repeats of the telomeric quadruplex.

Keywords

quadruplex DNA; telomere model; polynucleotide folding; loop structure; fluorescence; fluorescence quenching; quantum yield; fluorescence lifetime; 2-aminopurine; solvent accessibility

1. Introduction

1.1. Quadruplexes

Polynucleotides containing strings of contiguous guanine residues can associate to form quadruple stranded structures referred to as quadruplexes. There are many recent reviews of DNA quadruplexes that one may consult for details (e.g. (2–7)). For convenience, we provide a brief discussion of the structure of DNA quadruplexes below. These macromolecular assemblies consist of helical arrays of stacked planer, cyclic structures of four guanines linked by 8 hydrogen bonds involving the N1, N2, N7 and O6 atoms of the bases within an individual G-quartet. The O6 atoms within a quartet are directed toward the central cavity of the quadruplex and thereby form a coordination site that can accommodate a cation such as Na^+ or K^+ (Fig. 1).

Conformational diversity is one of the remarkable characteristics of quadruplexes. This plasticity results from a variety of chemical and physical variables. For example, the number

*j.chaires@louisville.edu; Tel: +502 852 1172.

of G-quartets comprising a stack may vary, the individual strands may be parallel, antiparallel or of mixed polarity, the loops connecting the quartets may be diagonal or lateral, the sequences flanking the stacks may differ, the N-glycoside bonds of the G residues may adopt *syn* or *anti* conformations, and the stabilizing cation may vary. The topological diversity of monomolecular quadruplex structures with three G-stacks is illustrated schematically in Fig. 2.

Although the structure of G-quartets was first described in 1962 (9), interest in quadruplex forming oligonucleotides has accelerated over the last twenty years. This may be attributed to the observation in 1989 (10) that telomeres (which provide a mechanism for complete chromosomal replication and protect chromosomal ends from degradation) consist of repeating tracts of G-rich sequences such as d(TTTTGGGG) in the protozoan *Oxytricha nova* and d(TTAGGG) in humans. In human chromosomal DNA, 200–300 bp of these sequences protrude as a single-stranded overhang from the 3′ end and studies with model oligonucletoides suggest that these sequences form a series of tandem quadruplexes (11). Subsequent investigators have shown that telomeres in vivo contain quadruplexes, and that quadruplex conformational changes may represent a key process in controlling chromosomal replication (12,13). T h e relatively facile ability to respond to environmental changes by undergoing conformational transformations (which stands in remarkable contrast to their high degree of thermal stability) suggests that quadruplex motifs may possess regulatory properties in other fundamental biological contexts, for example in cellular senescence and oncogenesis (14,15).

Bioinformatic analysis has revealed the presence of G-rich segments in parts of eukaryotic genomes in addition to those described above (16); several of these segments have been shown to be involved in controlling expression of a number of genes, including a variety of oncogenes as well as sequences involved in immunoglobulin switching (17). In addition, based on their putative regulatory roles, quadruplex-containing DNA segments are rational targets for drug development (7,18,19). Development of drugs targeted to specific quadruplex sequences requires an appreciation of subtle conformational differences likely to exist among different quadruplexes.

Interest in quadruplex oligonucleotides is also increasing in biotechnology. Some applications of quadruplex structures include molecular recognition (aptamers (20)), analytical applications (molecular sensors (21)), materials science (nanostructures), engineering (nanomachines), (22) and as drugs (19). Full development of the potential of each of these aspects of quadruplex science depends on understanding the conformational properties of quadruplexes and quadruplex assemblies, as well as their ability to undergo controlled conformational transitions.

X-ray crystallography and NMR methods continue to provide structures of a variety of specific quadruplexes (reviewed in (3,6)). However, these high resolution methods have proven not to be universally applicable. For example, NMR yielded an ensemble of conformers structures of a model of the 22-nt human telomeric sequence d[AGGG(TTAGGG)$_3$] (HuTel22) in the presence of Na^+ (1). This structure consists of an anti-parallel “basket” structure characterized by two lateral and one diagonal dTTA loops (Fig. 2). However, it was not possible to obtain a solution structure for HuTel22 in the presence of K^+ (the more physiologically relevant cation), presumably because of the presence of several conformational isomers. Interestingly, HuTel22 could be crystallized in the presence of K^+ (23). The resulting structure exhibits a parallel-stranded topology with the three dTTA loops packed against the quadruplex core (the “propeller” topology). However, several studies suggest that the all-parallel structure found in the crystal may not be the predominant solution structure ((8) and references therein). In fact, NMR solution

studies of related sequences in the presence of K^+ suggest the possibility that so-called hybrid-1 or hybrid-2 (3 parallel strands + 1 antiparallel strand) may be the preferred solution structure in the presence of this cation (24–26)

These examples provide a concrete basis for the importance of applying a variety of lower resolution techniques to test structural hypotheses, detect conformational changes and to compare unknown structures with known structures. Of these methods, the use of site-specific spectroscopic probes is particularly useful because of their ability to report specific rather than global structural differences brought about by mutation or changes in solution conditions. In general, fluorescent probes can serve as versatile, site-specific conformational reporters.

1.2. 2-Aminopurine (2AP), as a site-specific oligonucleotide structural probe

In contrast to polypeptides, for which the intrinsic fluorescence of the indole and phenolic side chains provide sensitive fluorescent reporters, the fluorescence quantum yield of the purine and pyrimidine building blocks of polynucleotides is too low to be analytically useful (except for the relatively rare Y base of found in t-RNA^{Phe}). Thus, it is necessary either to substitute a fluorescent purine or pyrimidine analog at the residue of interest or attach a probe molecule to the oligonucleotide. The adenine analog, 2-aminopurine (Fig. 3), has been applied in a large number of studies as a site-specific fluorescent reporter for polynucleotide studies. This fluorescent purine exhibits a number of desirable properties that render it a good probe molecule for polynucleotides. Among these are: (1) 2AP can form Watson-Crick H-bonds with thymidine, uracil or cytidine, thus inducing little or no structural perturbation when substituted for adenine; (2) 2AP can be relatively inexpensively incorporated into oligonucleotides using common solid phase synthetic methods; (3) the quantum yield of fluorescence is highly sensitive to environmental conditions and thus local changes in conformation; (4) theoretical and practical aspects of the photochemistry of 2AP, especially in the context of oligonucleotide structure, are well established. In particular, 2AP fluorescence tends to increase with solvent exposure and to decrease with base stacking. The interested reader is referred to two excellent recent studies focusing on the application of site-specific 2AP probes of RNA folding (27,28). These papers provide a comprehensive outline of the properties of 2AP in relation to oligonucleotide structure as well as a guide to recent studies involving 2AP-containing oligonucleotides.

In the following, we describe our use of 2AP as a probe of quadruplex folding. In these studies, we used the susceptibility of 2AP fluorescence to collisional quenching by acrylamide as a probe of adenine exposure present in loops or between tandem quadruplexes. Taken in conjunction with other studies, these fluorescence quenching experiments help distinguish between conformational models of a single quadruplex as well as tandem two-quadruplex models of human telomeric DNA.

1.3 Theoretical background for collisional quenching of fluorescence

Many excellent texts (for example (29) provide good summaries of biological applications of fluorescence. Fluorescence is defined as the emission of a photon from a singlet excited state to the ground state subsequent to absorption of a photon by a fluorophore. The fluorescence properties of a system are characterized by a number of parameters: excitation wavelength, emission wavelength, quantum yield (q) and lifetime of the excited state (τ_0). The quantum yield for fluorescence is defined as the ratio of photons emitted by fluorescence to photons absorbed. Alternatively, $q = k_f/\sum k_i$, where k_f is the rate of fluorescence emission and $\sum k_i$ represents the sum of rate constants for all mechanisms of loss of excitation energy. This expression shows explicitly the link between quantum yield and fluorescence lifetime.

Direct determination of *q* is generally not convenient; however, it is often sufficient to determine the relative quantum yield *F*, which is the emission intensity of the system measured under defined conditions. *F* is a function of the instrument (intensity of excitation source, sensitivity of the detection system etc.) as well as the conditions of the measurement (fluorophore concentration, temperature and solution conditions). *F* is most accurately obtained from integration over the wavelengths of the emission envelope; however, it may be adequate to determine *F* as the emission intensity at the emission wavelength maximum. Depending on the instrument, *F* may be given in photons/sec or in arbitrary units.

The excited state lifetime is the average time that a fluorophore spends in the excited state before emitting a photon. For a homogeneous system, fluorescence decay consists of a single exponential process. In general, for fluorophores in a heterogeneous environment the decay of fluorescence consists of multiple exponentials as defined by the relationship $F(t)/F_0 = \sum \alpha_i \cdot \exp(-t/\tau_{0,i})$ where α_i is the amplitude of the fluorescence intensity for species *i* and $\tau_{0,i}$ is the lifetime for that species. Fluorescence lifetimes are generally in the sub-nanosecond to nanosecond time range and require specialized instrumentation for determination.

For many fluorophores, the measurable characteristics of fluorescence such as emission maximum, *q* and τ_0 are sensitive to the local environment of the fluorophore. However, for 2AP, it turns out that the emission maximum is not very sensitive to its environment, but *q* and τ_0 are environmentally quite sensitive. Often the structural basis of these variations in τ_0 and *q* can be quite subtle. For example, 2AP fluorescence is enhanced by cooling (indicating the importance of conformational motion), quenched by base stacking, enhanced by energy transfer from neighboring adenine, and strongly quenched by collision with neighboring G residues. In addition, 2AP emission is quenched by solutes such as acrylamide that quenches by collision with the excited state fluorophore. As described below, the action collisional quenchers is generally described by the Stern-Volmer equation or modifications of it.

1.4 Stern-Volmer quenching

Classical Stern-Volmer quenching (also referred to as dynamic quenching) can be explained by a simple mechanism in which the quenching agent, Q, collides with an excited fluorophore F*. In this type of quenching, the excited state energy is lost when the excited fluorophore collides with Q and forms a transient encounter complex as depicted in scheme 1:

$$F^* + Q \leftrightarrow (F^* \cdots Q) \leftrightarrow (F \cdots Q) \rightarrow F + Q + \text{thermal energy}. \quad (1)$$

Formation of (F*·····Q) depends on the diffusion rate constant for F* and Q, their concentrations and the efficiency of the quenching process. For a single fluorescent species in a homogeneous environment, the degree of quenching increases with increasing [Q] according to the Stern-Volmer relationship:

$$F_0/F_Q = 1 + K_{SV}[Q] = 1 + \tau_0 k_q [Q] = 1 + \tau_0 f_Q k_0 [Q] \quad (2)$$

where F_0 is the fluorescence observed in the absence of quencher, F_Q is the fluorescence observed in the presence of quencher at concentration [Q], K_{SV} is the Stern-Volmer quenching coefficient, τ_0 is the lifetime of the excited state in the absence of Q, $k_q$is the bimolecular quenching constant, f_Q is the efficiency of quenching, and k_0 is the (diffusion-controlled) bimolecular collisional rate constant. From Eq. 2, a plot of F_0/F_Q *versus* [Q] is linear with a slope K_{SV} from which f_0 can be extracted if τ_0 and k_0 are known. The former

may be available in the literature or measured directly and the latter can be estimated from the Smoluchowski equation (Note 1). Under defined conditions for a given quenching agent and a homogeneous fluorescent system, f_0 is related to the accessibility of F* to Q. In the absence of known values of τ_0 and k_0, the relative accessibility of F* to Q can qualitatively be assessed by comparing values of K_{SV} measured for the same fluorophore measured under different solvent conditions. Hence, under ideal circumstances, collisional quenching can provide insight into the relative degree of exposure of a fluorophore to solvent.

Experience has shown that the Stern-Volmer plot often is not linear but exhibits either a concave or convex relationship with respect to [Q]. A non-linear Stern-Volmer plot indicates a heterogeneous fluorescing system. This heterogeneity may arise either from fluorophores with different k_0, f_0 and/or τ_0 values or from formation of static complexes with Q. In systems with a single fluorophore (such as the quadruplexes under consideration in this article) downward curvature is interpreted to indicate that the fluorophore experiences more than one micro-environment. Such a heterogeneous quenching system can in general be described by Eq. 3:

$$F_0/F_Q = \sum_{i=1}^{n} \frac{f_i}{1+K_{SV,i}[Q]}, \qquad \text{Eq. 3}$$

where $K_{SV,i}$ is the quenching constant for the ith species and $f_i$is the fractional contribution of the ith species to the total fluorescence. Explicitly for a two-component system:

$$F_0/F_Q = \frac{f_1}{1+K_{SV,1}[Q]} + \frac{1-f_1}{1+K_{SV,2}[Q]}. \qquad \text{Eq. 4}$$

Eftink (30) has shown that if $K_{SV,1} \geq 4 \cdot K_{SV,2}$, the F_0/F_Q plot will exhibit visible downward curvature. Fitting the data to Eq. 4 by non-linear least squares allows determination of the optimal values of the parameters f_1, $K_{SV,1}$ and $K_{SV,2}$ (although see Note 2).

Upward curvature is generally interpreted to indicate formation of both static and dynamic (collisional) complexes (Note 3). This case will not be treated here; the interested reader is referred to a standard text book for details regarding interpretation and quantitative analysis of upwardly curving Stern-Volmer plots.

Summary of fluorescence properties of 2AP—The fluorescence properties of 2AP in water are as follows: emission involves a $\pi^* \rightarrow \pi$ transition, with an excitation maximum of ~305 nm and emission maximum at ~370 nm, q = 0.7; fluorescence decay is mono-exponential with τ_0 = 12 ns (31). The emission maximum is relatively insensitive to solvent polarity and q is not affected by pH but is strongly dependent on temperature. In the context of an oligonucleotide, q is strongly influenced by nearest neighbors and by base stacking. Quenching of 2AP fluorescence by acrylamide gives a Stern-Volmer plot with slight upward curvature which has been attributed to a weak static quenching component at high [acrylamide]. K_{SV} for acrylamide quenching of 2AP is ~28 M^{-1} at 10 °C and increases to ~58 M^{-1} at 70 °C.

2. Materials

2.1 Preparation of buffers, acrylamide solutions and DNA

1. A variety of different buffer systems have been used to study quadruplexes. For the studies described in Fig. 3, BPES and BPEK buffers consisting of 6 mM Na_2HPO_4, 2 mM NaH_2PO_4, 1 mM Na_2EDTA, 185 mM NaCl or KCl, pH 7.1 were used.
2. Concentrated stock solutions (4–6 M acrylamide) can be prepared by carefully adding the desired amount of high-quality acrylamide to a tared volumetric flask followed by adding the appropriate buffer to volume. Alternatively, concentrated acrylamide solutions are available commercially from a variety of laboratory suppliers. These solutions are generally prepared in water; thus the buffer concentration will change during the titration if such solutions are used for the titrations. Acrylamide solutions are susceptible to degradation and should be stored at 4 °C in a foil-wrapped container to protect from exposure to light. (See Note 4 regarding toxicity and disposal of acrylamide).
3. Desalted, lyophylized deoxyoligonucleotides with single dA residues substituted serially with 2AP were purchased from commercial sources: (Oligos Etc, http://www.oligosetc.com/ index.phpor or IDT, http://www.idtdna.com/home/home.aspx). The oligonucleotides were used without further purification and were dissolved in a small volume of an appropriate buffer to give a stock solution of ~500–1000 μM. Oligonucleotide concentrations were determined from the absorbance at 260 nm using absorption coefficients supplied by the manufacturer (See Note 5).

3. Methods

3.1 Acrylamide titrations

1. The fluorescence measurements were carried out with a JASCO FP-6500 fluorometer equipped with a peltier temperature controller and a magnetic mixer.
2. Oligonucleotides were excited at 305 nm and emission spectra were measured from 320 nm to 420 nm. Excitation and emission slits were set to 5 nm.
3. The fluorometer is allowed to stabilize for ~ 30 min after turning it on.
4. Add buffer to fluorescence cuvette; equilibrate with stirring for several minutes to achieve a constant temperature in the cuvette. We use a 1 × 1 cm quartz fluorescence cuvette that can accommodate 2.4–3.0 ml of sample.
5. Record and store fluorescence baseline of the buffer. Many fluorometers allow digital recording of spectra and signal averaging by recording multiple spectra to increase signal:noise if necessary.
6. Add oligonucleotide from the stock solution to give a reasonable signal at the emission maximum for 2AP of 372 nm. Depending on the fluorometer, the final oligo concentration is 0.2–2 μM in 2AP equivalents. Check the oligo concentration by determining its absorbance at 260 nm. The absorbance of the solution used for fluorescence measurements should be ≤ 0.1 to minimize inner filter effects (29).
7. Record and store the emission spectrum of 2AP-oligo without added acrylamide.
8. Add an aliquot of the stock acrylamide solution to give a final concentration of 0.02–0.1 M. Ensure that mixing is adequate; record emission spectrum.

9. Continue serial addition of the stock acrylamide solution to give points encompassing a range of acrylamide concentrations between 0 and ~0.8 M. Record the emission spectrum after each addition.

3.2 Data analysis

1. Subtract buffer blank spectrum from each experimental spectrum.
2. Correct the spectra for dilution by multiplying by the appropriate dilution factor.
3. Plot F_0/F_Q determined at the emission maximum (~370 nm) vs. [acrylamide] (Stern-Volmer plot).
4. Fit the data points to an appropriate analytical expression: Eq. 1 if the Stern-Volmer plot is linear or Eq. 4 if the S-V plot shows downward curvature. We use the non-linear least squares module in the computer program Origin 7.0 (OriginLab, Northampton, MA; http://www.originlab.com/)

3.3 Interpretation of data

Here we provide two examples of 2AP-acryamide quenching data used by our group to assess the degree of exposure of individual dA residues in two models of the human telomeric DNA sequence. In the first study, Li et al. (8) compared the acrylamide quenching curves of HuTel22 in sodium and potassium buffers. The purpose of this study was to compare the exposure of the loop adenines in solution with the predicted exposures assessed from the solution structure of HuTel22 in Na^+ (antiparallel basket) determined by NMR and the structure of the same oligonucleotide determine in K^+ by x-ray crystallography (all parallel propeller structure). The two topographical arrangements have very different loop geometries and hence different environments for the loop adenines. In the basket structure, A1, A13 and A19 are stacked upon G-tetrads; A7 is unstacked. This is consistent with the apparent quantum yields (F_0 values) of the 2AP substituted oligonucleotides in Fig. 3 and summarized in Table 1: A7 > A19 > A1 ≈ A13. It is well established that 2AP fluorescence is strongly quenched by nearby G residues, probably via an electron-transfer mechanism. The close proximity of A1, A13 and A19 to Gs in the Patel structure may account for some or all of these quenching effects.

As described above, provided appropriate τ_0 values are known, collisional quenching data can provide information about environmental heterogeneity at the positions of substitution. According to the Stern-Volmer model (Eq. 1), a single fluorophore with a uniform microenvironment exhibits a linear relationship between F_0/F and [Q]. Differences in K_{SV} between different single probe residues, each in a homogeneous microenvironment may result either from alterations in k_0, τ_0 or both (Eq. 1). Clearly, without prior knowledge of τ_0 for different single 2AP substitutions, it is impossible to correlate K_{SV} directly with the accessibility of the reporter group to solvent. Kimura et al. (32) have determined that in Na^+ or K^+, the fluorescence decay curves of HuTel22 with serial dA → 2AP substitutions, consist of a single exponential with lifetimes (τ_0) of 0.54, 0.34 and 0.35 ns for AP7, AP13 and AP19, respectively (32,33). This implies that, to a close approximation, the observed alterations in K_{SV} result from alterations in the k_0, which varies with the accessibility of the excited state fluorophore to the quenching agent at constant temperature and viscosity.

The quenching curves shown in Fig. 3 B and D are clearly concave with respect to [acrylamide]. In the case of the Na^+ structure the excited state 2AP must experience at least two distinct microenvironments: one that is relatively accessible to Q and one that is shielded from Q. The structural basis of these differences is unclear; however, given that NMR indicates a single global fold (the basket structure) the structural heterogeneity

probably results from highly localized, nanosecond fluctuations in positioning of the adenine that are confined to the respective loop regions.

To put the analysis on a more quantitative basis, we fit the quenching curves to a two-state model (Eq. 3 with $n = 2$), even though we realized that such a model likely is an oversimplification. The resulting best fit parameters ($K_{SV,1}$, $K_{SV,2}$ and f_1) are summarized in Table 1. $K_{SV,1}$ varies from 6.8 M^{-1} to 12.8 M^{-1}, K_{SV},2 varies from 0 to 0.2 M^{-1}, and f_1 varies between 0.52 and 0.86. This analysis suggests that in Na^+, AP7 and AP19 are nearly homogeneous with respect to their accessibility to acrylamide quenching ($f_1 \approx 0.86$), whereas a significant fraction of the AP1 and AP13 bases are relatively inaccessible to acrylamide quenching (32% and 42%, respectively). If the K_{SV} parameters in Table 1 in Na^+ are divided by the τ_0 values above, the bimolecular collisional constant k_0 = 13.6, 20.1 and 21.6 M^{-1} ns^{-1} for AP7, AP13 and AP19, respectively for the solvent-exposed residues, and approximately 100-fold less for the inaccessible fractions. The results are consistent with our earlier conclusions derived from the NMR structure of HuTel22 in Na^+ that A13 is packed within the diagonal loop at one end of the structure while A7 and A19 are in more exposed regions in the lateral loops at opposite ends of the structure. However, the heterogeneity apparent in the f_1 values suggests some flexibility in the diagonal loop such that on average, about half of the residues are relatively solvent accessible.

For K^+, all quenching curves also display downward curvature as shown in Fig. 3D, indicative of local environmental heterogeneity at the sites of substitution as described above with Na^+. When these data were analyzed by the 2-state model (Eq. 4), only A13 exhibited nearly equal fractions of relatively accessible and inaccessible states (f_1 = 0.55 and f_2 = 0.45). For the other substitutions, only 10–20% of the 2AP residues are relatively inaccessible to acrylamide, suggesting a relatively homogeneous environment. Notably, the K_{SV} parameters associated with the accessible population of states are all the approximately the same ($K_{SV} \approx 9.0$–9.5 M^{-1}). Since the requisite τ_0 values are not available in K^+, it is not possible to directly relate these K_{SV} values to residue accessibility. However, f_1 values (for A13) that are markedly < 1.0 indicate that a significant fraction of the residues reside in a microenvironment that is inaccessible to acrylamide. This leads to our previous conclusion that the structure of HuTel22 in K^+ solutions is not the propeller structure, in which all loop adenines (A7, A13 and A19) are in equivalent environments.

In a second example, Petraconne et al. (34) correlated emission intensities and acrylamide quenching data with solvent accessible surface areas calculated for several different models of a 50-nt oligonucleotide $d(TTAGGG)_8TT$. This sequence models eight repeats of the TTAGGG human telomere sequence and consists of two tandem quadruplexes. Molecular dynamics was used to model various combinations of hybrid-1, hybrid-2 and propeller structures, and the solvent accessible surface area (SASA) of each dA residue was calculated from the final 4 ns of the molecular dynamics trajectory. The authors compared the SASA with the observed F_0/F values at 0.6 M acrylamide for a series of oligonucleotides in which each of the eight loop dA residues was individually substituted with 2AP. They concluded that one combination of topologies (hybrid-1-hybrid-2) showed the best correlation between SASA and accessibility to acrylamide.

In summary, the two studies discussed above show how fluorescence emission and fluorescence quenching measurements can be used to distinguish unambiguously between closely related structural models of G-quadruplexes. In common with similar studies, it is possible to determine best fitting values of parameters such as K_{SV} which may be related to solvent accessibility and hence can be correlated with various structural models. However, because K_{SV} is a product of at least three independently variable physical parameters (τ_0, k_0 and f_0), and because of the difficulty of determining all of them independently from

quenching curves, K_{SV} values should be interpreted cautiously with respect to specific structures. Nevertheless, we and others have demonstrated that even in the absence of a rigorous quantitative interpretation of these variables, when high resolution model structures are available from which predictions regarding accessibility of dA residues can be made, the fluorescence properties of 2AP can be a valuable aid in model discrimination, especially when taken in conjunction with other biophysical measurements such as sedimentation.

4. Notes

1. The value of k_0, the diffusion-limited bimolecular collisional rate constant can be estimated from the Smoluchowski equation: $k_0 = 4\pi DR_0N'$ where D and R_0 are the sum of the diffusion coefficients and molecular radii of the quencher and fluorophore and N' is Avogadro's number divided by 1000. The diffusion constants can be calculated from the Stokes-Einstein equation $D_i = k_BT/(6\pi R\eta)$ where k_B is the Boltzmann constant, T is the absolute temperature, R is the molecular radius of the species, and η is the solvent viscosity (30).
2. Non-linear least squares analysis of the fitting of $K_{SV,1}$, $K_{SV,2}$ and f_1 to equation 3 with $n = 1$ or $n=2$ revealed that the optimized parameters are highly correlated (e.g. for the data sets shown, the covariance between any pair of parameters was ± ~0.9 as determined from the covariance matrix). Thus, the parameters may not represent unique values, but rather should be regarded as descriptive values that can reproduce the data within experimental error. In addition, even though the fit to the experimental data points is generally quite good as judged by the SSR and residual plots, this in itself is not sufficient to justify the use of the 2-state model.
3. A modified Stern-Volmer equation has been used to describe quenching curves with upward curvature resulting from static quenching. This relationship is $F_0/F = (1 + K_{SV}[Q])\cdot \exp(V[Q])$, where V is the volume surrounding the fluorophore in which one or more quencher molecules reside at the instant of excitation (the so-called "active volume element") (30).
4. Acrylamide is a known human neurotoxin and suspected carcinogen. It is readily absorbed through the skin and by inhalation. Please consult the appropriate material data safety sheet (http://www.jtbaker.com/msds/englishhtml/A1550.htm) for details on hazards, treatment for exposure, and procedures for cleanup of accidental spilling. Your institutional regulations should be consulted prior to disposal of acrylamide.
5. The absorption coefficient for 2AP at 305 nm has been reported to be 6000 M^{-1} cm^{-1}. For 2AP incorporated into an oligonucleotide, the absorption coefficient at 260 nm is 1700 M^{-1} cm^{-1} (35,36)

Acknowledgments

Supported by grant CA35635 from the National Cancer Institute.

References

1. Wang Y, Patel DJ. Solution structure of the human telomeric repeat d[$AG_3(T_2AG_3)_3$] G-tetraplex. Structure 1993;1:263–282. [PubMed: 8081740]
2. Davis JT. G-quartets 40 years later: From 5'-GMP to molecular biology and supramolecular chemistry. Ang. Chem. Inter. Ed 2004;43:668–698.
3. Burge S, Parkinson GN, Hazel P, Todd AK, Neidle S. Quadruplex DNA: sequence, topology and structure. Nucleic Acids Res 2006;34:5402–5415. [PubMed: 17012276]

4. Dai J, Carver M, Yang D. Polymorphism of human telomeric quadruplex structures. Biochimie 2008;90:1172–1183. [PubMed: 18373984]
5. Huppert JL. Four-stranded nucleic acids: structure, function and targeting of G-quadruplexes. Chem. Soc. Rev 2008;37:1375–1384. [PubMed: 18568163]
6. Lane AN, Chaires JB, Gray RD, Trent JO. Stability and kinetics of G-quadruplex structures. Nucleic Acids Res 2008;36:5482–5515. [PubMed: 18718931]
7. Neidle S, Parkinson GN. Quadruplex DNA crystal structures and drug design. Biochimie 2008;90:1184–1196. [PubMed: 18395014]
8. Li J, Correia JJ, Wang L, Trent JO, Chaires JB. Not so crystal clear: the structure of the human telomere G-quadruplex in solution differs from that present in a crystal. Nucleic Acids Res 2005;33:4649–4659. [PubMed: 16106044]
9. Gellert M, Lipsett MN, Davies DR. Helix formation by guanylic acid. Proc. Natl. Acad. Sci. U.S.A 1962;48:2013–2018. [PubMed: 13947099]
10. Williamson JR, Raghuraman MK, Cech TR. Monovalent cation-induced structure of telomeric DNA: the G-quartet model. Cell 1989;59:871–880. [PubMed: 2590943]
11. Wright WE, Tesmer VM, Huffman KE, Levene SD, Shay JW. Normal human chromosomes have long G-rich telomeric overhangs at one end. Genes Dev 1997;11:2801–2809. [PubMed: 9353250]
12. Paeschke K, Simonsson T, Postberg J, Rhodes D, Lipps HJ. Telomere end-binding proteins control the formation of G-quadruplex DNA structures in vivo. Nat. Struct. Mol. Biol 2005;12:847–854. [PubMed: 16142245]
13. Schaffitzel C, Berger I, Postberg J, Hanes J, Lipps HJ, Pluckthun A. In vitro generated antibodies specific for telomeric guanine-quadruplex DNA react with *Stylonychia lemnae* macronuclei. Proc. Natl. Acad. Sci. U.S.A 2001;98:8572–8577. [PubMed: 11438689]
14. Collado M, Blasco MA, Serrano M. Cellular senescence in cancer and aging. Cell 2007;130:223–233. [PubMed: 17662938]
15. Ruzankina Y, Asare A, Brown EJ. Replicative stress, stem cells and aging. Mech. Ageing Dev 2008;129:460–466. [PubMed: 18462780]
16. Huppert JL, Balasubramanian S. G-quadruplexes in promoters throughout the human genome. Nucleic Acids Res 2007;35:406–413. [PubMed: 17169996]
17. Duquette ML, Handa P, Vincent JA, Taylor AF, Maizels N. Intracellular transcription of G-rich DNAs induces formation of G-loops, novel structures containing G4 DNA. Genes Dev 2004;18:1618–1629. [PubMed: 15231739]
18. Han H, Hurley LH. G-quadruplex DNA: a potential target for anti-cancer drug design. Trends Pharmacol. Sci 2000;21:136–142. [PubMed: 10740289]
19. Teng Y, Girvan AC, Casson LK, Pierce WM Jr, Qian M, Thomas SD, et al. AS1411 alters the localization of a complex containing protein arginine methyltransferase 5 and nucleolin. Cancer Res 2007;67:10491–10500. [PubMed: 17974993]
20. Shafer RH, Smirnov I. Biological aspects of DNA/RNA quadruplexes. Biopolymers 2000;56:209–227. [PubMed: 11745112]
21. Juskowiak B. Analytical potential of the quadruplex DNA-based FRET probes. Anal. Chim. Acta 2006;568:171–180. [PubMed: 17761258]
22. Alberti P, Bourdoncle A, Sacca B, Lacroix L, Mergny JL. DNA nanomachines and nanostructures involving quadruplexes. Org. Biomol. Chem 2006;4:3383–3391. [PubMed: 17036128]
23. Parkinson GN, Lee MP, Neidle S. Crystal structure of parallel quadruplexes from human telomeric DNA. Nature 2002;417:876–880. [PubMed: 12050675]
24. Ambrus A, Chen D, Dai J, Bialis T, Jones RA, Yang D. Human telomeric sequence forms a hybrid-type intramolecular G-quadruplex structure with mixed parallel/antiparallel strands in potassium solution. Nucleic Acids Res 2006;34:2723–2735. [PubMed: 16714449]
25. Luu KN, Phan AT, Kuryavyi V, Lacroix L, Patel DJ. Structure of the human telomere in K^+ solution: an intramolecular (3 + 1) G-quadruplex scaffold. J. Am. Chem. Soc 2006;128:9963–9970. [PubMed: 16866556]
26. Xu Y, Noguchi Y, Sugiyama H. The new models of the human telomere d[AGGG(TTAGGG)$_3$] in K^+ solution. Bioorg. Med. Chem 2006;14:5584–5591. [PubMed: 16682210]

27. Ballin JD, Bharill S, Fialcowitz-White EJ, Gryczynski I, Gryczynski Z, Wilson GM. Site-specific variations in RNA folding thermodynamics visualized by 2-aminopurine fluorescence. Biochemistry 2007:13948–13960. [PubMed: 17997580]

28. Ballin JD, Prevas JP, Bharill S, Gryczynski I, Gryczynski Z, Wilson GM. Local RNA conformational dynamics revealed by 2-aminopurine solvent accessibility. Biochemistry 2008;47:7043–7052. [PubMed: 18543944]

29. Lakowicz, JR. Principles of Fluorescence Spectroscopy. New York: Plenum Press; 1999.

30. Eftink, MR. Topics in Fluorescence Spectroscopy. Lakowicz, JR., editor. Vol. Vol. 2. New York: Plenum Press; 1991. p. 53-126.

31. Hardman SJ, Botchway SW, Thompson KC. Evidence for a nonbase stacking effect for the environment-sensitive fluorescent base pyrrolocytosine-comparison with 2-aminopurine. Photochem. Photobiol 2008;84:1473–1479. [PubMed: 18513237]

32. Kimura T, Kawai K, Fujitsuka M, Majima T. Fluorescence properties of 2-aminopurine in human telomeric DNA. Chem. Commun 2004:1438–1439.

33. Kimura T, Kawai K, Fujitsuka M, Majima T. Detection of the G-quadruplex-TMPyP4 complex by 2-aminopurine modified human telomeric DNA. Chem. Commun 2004;4:401–402.

34. Petraccone L, Trent JO, Chaires JB. The tail of the telomere. J. Am. Chem. Soc 2008;130:16530–16532. [PubMed: 19049455]

35. Johnson NP, Baase WA, Von Hippel PH. Low-energy circular dichroism of 2-aminopurine dinucleotide as a probe of local conformation of DNA and RNA. Proc. Natl. Acad. Sci. U.S.A 2004;102:3426–3431. [PubMed: 14993592]

36. Smagowicz J, Wierzchowski KL. Lowest excited states of 2-aminopurine. J. Luminescence 1974;8:210–232.

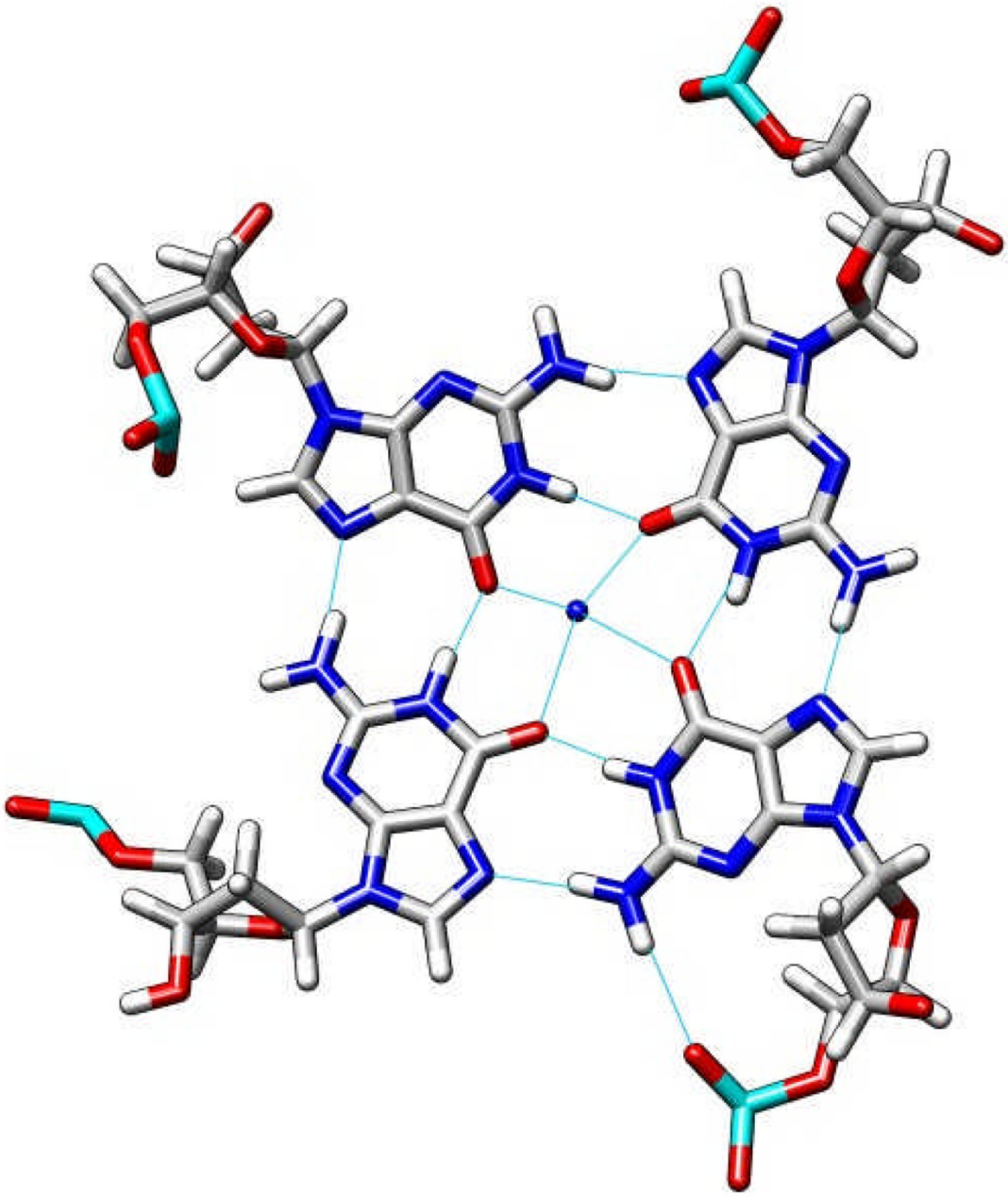

Fig. 1.

G-quartet showing H-bonding pattern and coordinated sodium ion in center. The figure shows a single G-quartet and is based on the coordinates of HuTel22 in PDB file 143D (1). The hydrogen bonding pattern is shown by the thin lines connecting the N and O atoms. The D-ribosyl phosphate moieties are shown on the periphery of the

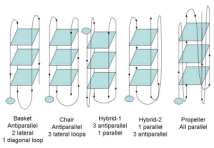

Fig. 2.

Schematic diagram of potential folding topographies of unimolecular quadruplexes. The Na^+ form of HuTel22 has been shown to exist in solution mainly in the form of an antiparallel basket (1). In the presence of K^+, HuTel22 in crystals is an all-parallel “propeller” structure (23). In K^+ solution, NMR and other physical studies indicate that HuTel22 is present as a mixture of different conformers (4,8). The circle represents the 5′ end of the oligonucleotide.

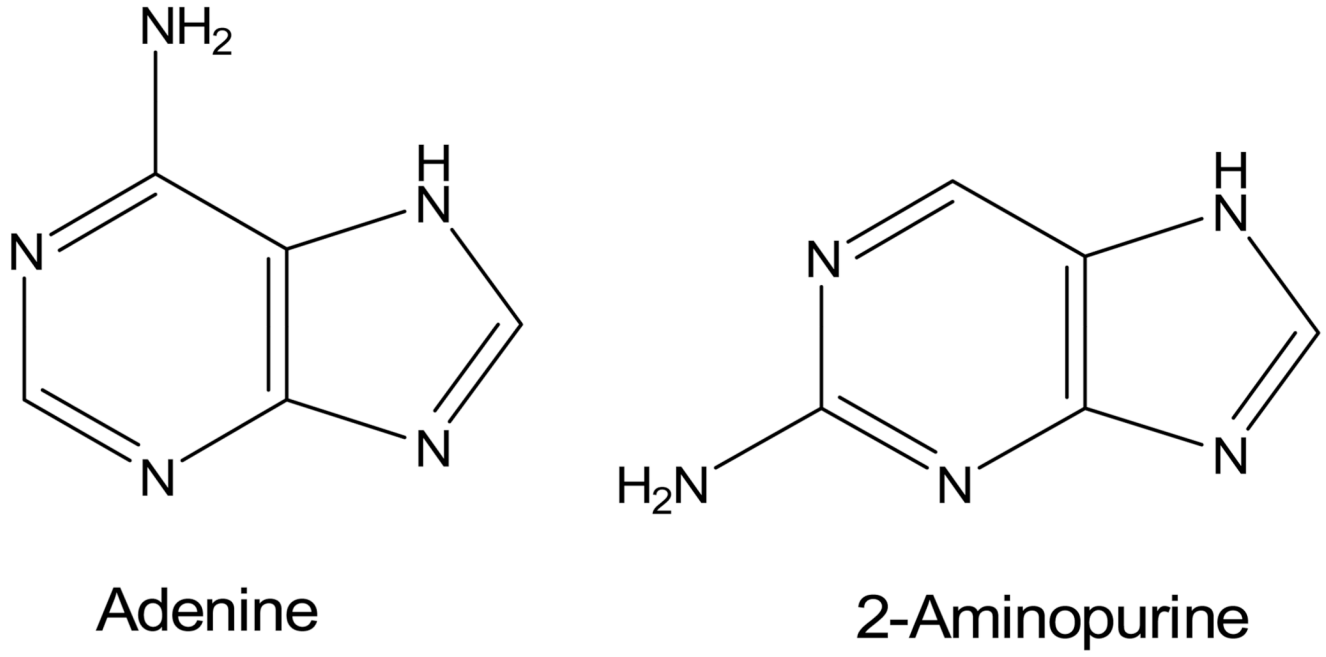

Fig. 3.
Structures of adenine and 2-aminopurine

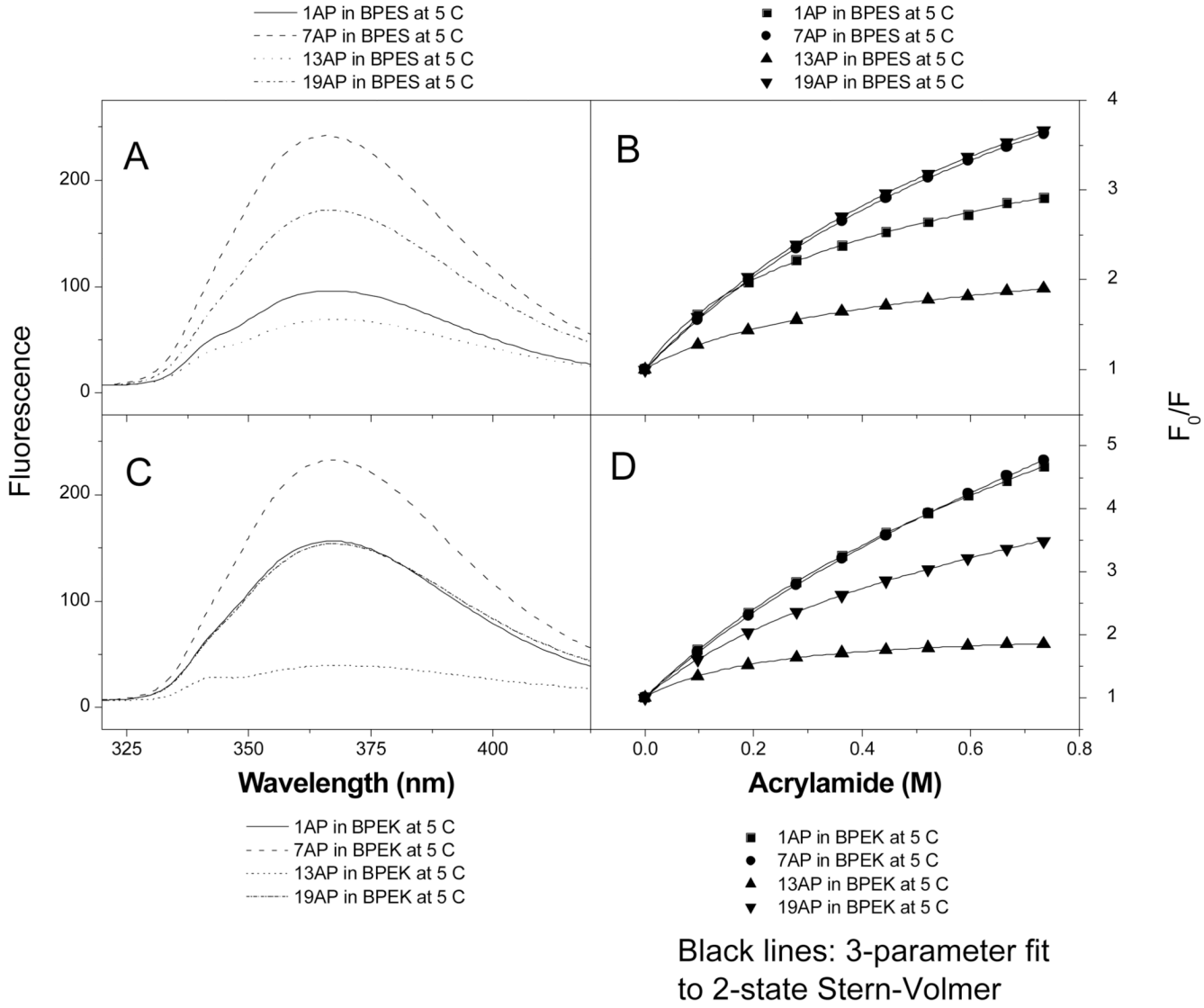

Fig. 4.

Emission spectra (panels A and C) and fluorescence quenching curves (panels B and D) for HuTel22 measured in the presence of Na^+ or K^+ at 5 °C. The lines were drawn in the Stern-Volmer plots using the optimized parameters $K_{SV,1}$, $K_{SV,2}$ and f_1 given in Table 1 and determined by non-linear least fitting of the quenching data to Eq. 4 as described in the text. The data are re-plotted from reference (8).

Table 1

Fluorescence intensities and optimized Stern-Volmer parameters for acrylamide quenching of HuTel22 for a two-state model. This model assumes that in each oligonucleotide, 2AP is characterized either by state 1 (more exposed to Q) or state 2 (less exposed to Q). The data in Fig. 3 were fit to Eq. 4 using the non-linear least squares fitting module of the program Origin 7.0. The error values show the standard deviation of the fit of the individual data sets as calculated from the diagonal elements of the error matrix.

Na^+ buffer	SASA (Å^2)[a]	Relative F_0 at 370nm[b]	$K_{SV,1}$ (M^{-1})	$K_{SV,2}$ (M^{-1})	f_1	1 - f_1
1AP	102	2.4	12.84±0.86	0.23±0.06	0.68±0.02	0.32
7AP	107	6.0	7.19±0.09	−0.01±0.03	0.86±0.01	0.14
13AP	38	1.7	6.84±0.41	0.12±0.03	0.52±0.02	0.48
19AP	25	4.3	7.57±0.17	−0.02±0.05	0.86±0.01	0.14
K^+ buffer						
1AP	196	3.9	9.65±0.17	0.18±0.05	0.88±0.01	0.12
7AP	98	5.8	9.07±0.25	0.39±0.10	0.88±0.01	0.12
13AP	91	1.0	9.01±0.19	−0.05±0.01	0.55±0.01	0.45
19AP	96	3.8	9.44±0.20	0.29±0.03	0.77±0.01	0.23
2AP alone	269	192[d]	37.65±0.37[e]	-	101.5±2.2[f]	-

[a] SASA: solvent accessible surface area of the 2AP moiety calculated from the NMR structure of HuTel22 (Protein Data Bank entry 143D (1)) in Na^+ and the crystal structure in K^+ (PDB entry 1KF1 (23)).

[b] Normalized with respect to F_0 = 40 arbitrary units for 13AP in K^+.

[d] Determined for 2AP and 13AP in BPEK at 25 °C.

[e] Determined at 25°C in 50 mM KOAc, 5 mM $Mg(OAc)_2$ by Ballin et al. (27).

[f] The Stern-Volmer plot showed upward curvature, indicative of static quenching (27).